Supporting Information:

Observation of Parallel Intersystem Crossing and Charge Transfer-state Dynamics in [Fe(bpy)$_3$]$^{2+}$ from Ultrafast 2D Electronic Spectroscopy

Angela Lee,[†] Minjung Son,[†,§] Mawuli Deegbey,[‡] Matthew D. Woodhouse,[¶]

Stephanie M. Hart,[†,‖] Hayden F. Beissel,[¶] Paul T. Cesana,[†] Elena Jakubikova,[‡]

James K. McCusker,[*,¶] and Gabriela S. Schlau-Cohen[*,†]

[†]*Department of Chemistry, Massachusetts Institute of Technology, Cambridge, MA 02139*

[‡]*Department of Chemistry, North Carolina State University, Raleigh, NC 27695*

[¶]*Department of Chemistry, Michigan State University, East Lansing, MI 48824*

[§]*Current Address: Department of Chemistry, Boston University, 590 Commonwealth Ave, Boston, MA 02215*

[‖]*Current Address: Department of Chemistry, University of California, Berkeley, Berkeley, CA 94720*

E-mail: jkm@chemistry.msu.edu; gssc@mit.edu

Contents

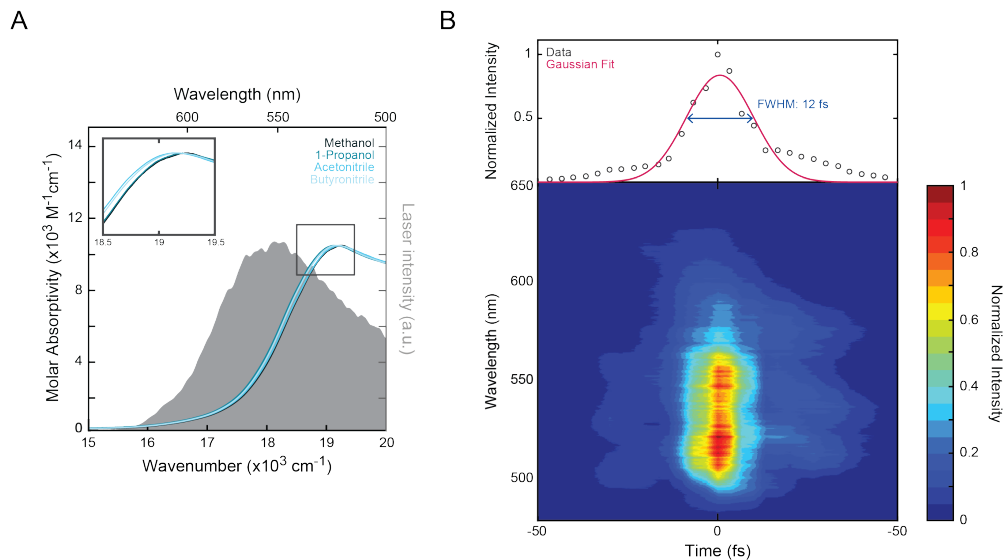# 1 Setup and Sample Characterization

1.1 Pulse characterization

Figure S1: Pulse characterization of the 2DES experiment. (A) Linear absorption spectra of $[\text{Fe(bpy)}_3]^{2+}$ in methanol, 1-propanol, acetonitrile, and butyronitrile (blue lines). The region from $18,500 - 19,500$ cm^{-1} is enlarged in the insert to show the minor differences amongst the spectra in the solvents. The spectrum used for the ultrabroadband 2D electronic spectroscopy (2DES) experiment outlined in the main text is denoted in gray. (B) The TG-FROG trace of the pulse used for the 2DES experiment. The top panel shows the temporal profile, along with the gaussian fit to determine the full-width at half maximum.
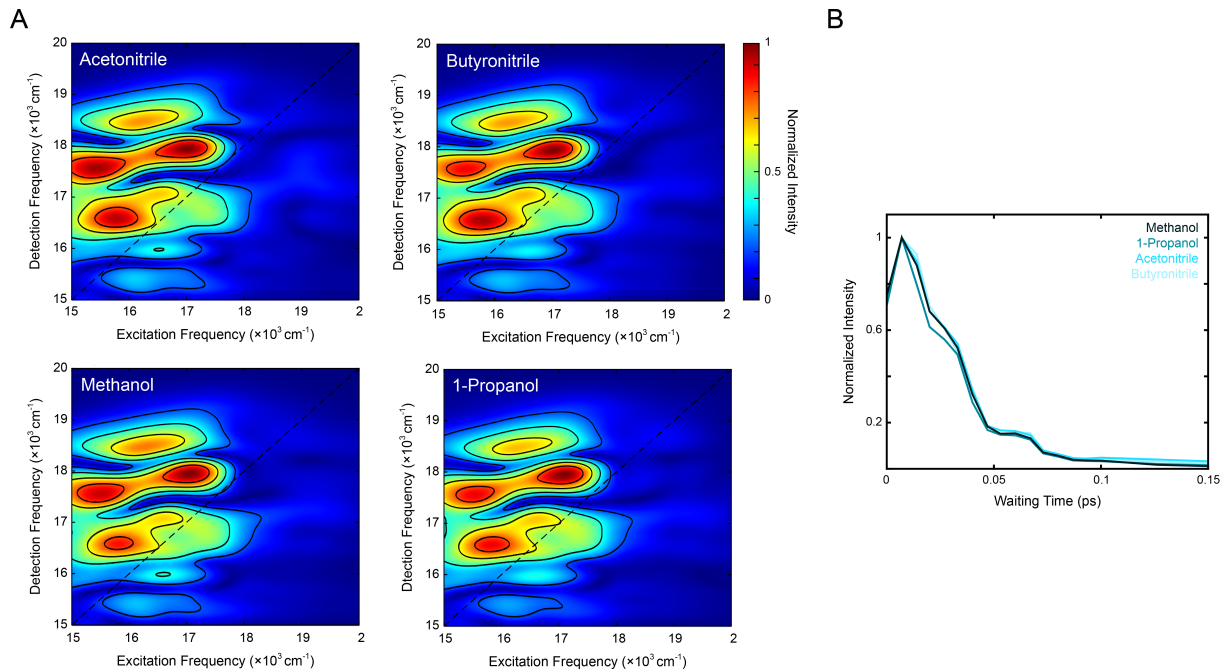
Figure S2: Characterization of the nonresonant response in the sample. (A) Normalized absolute value 2DES spectra of the non-resonant response of acetonitrile, butyronitrile, methanol, and 1-propanol at waiting time $T = 27$ fs. Contour lines are drawn at 25% intervals. (B) Intensity trace of the non-resonant response, normalized, in each solvent (purple lines) as a function of waiting time T. The trace was integrated over $\omega_\tau = 15,000 - 20,000$ cm^{-1} and $\omega_t = 15,000 - 20,000$ cm^{-1}.

1.2 Phasing via projection-slice theorem

A

B
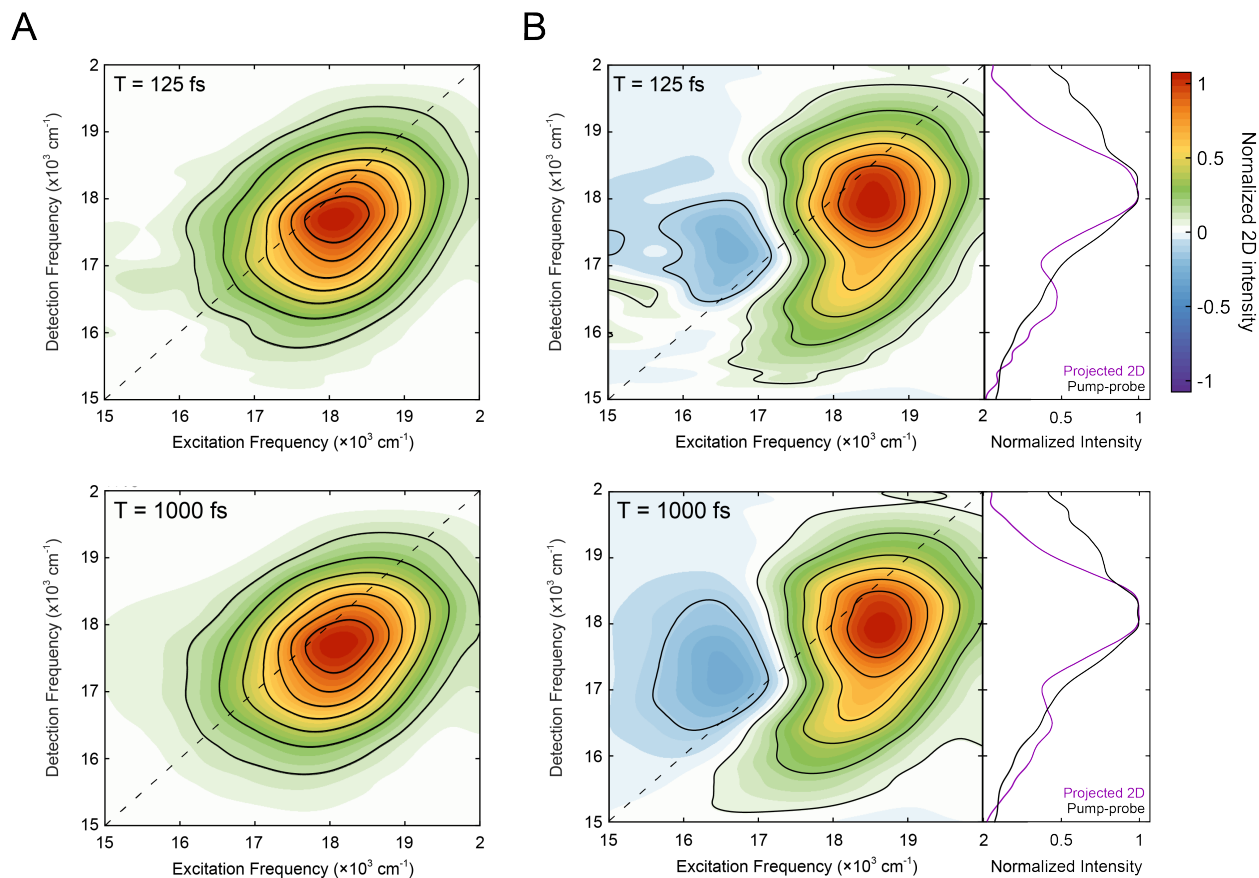

Figure S3: 2D projection traces onto the detection axis, used for phased data. The normalized 2DES absolute value spectrum of $[Fe(bpy)_3]^{2+}$ in methanol (A) at waiting times $T = 125$ fs and $T = 1000$ fs (top and bottom, respectively). (B) The normalized phased data at the same time points as in (A). The 2D spectrum is projected along the emission frequency axis (magenta line) and compared to the pump-probe spectrum (black line) and shown on the far right.
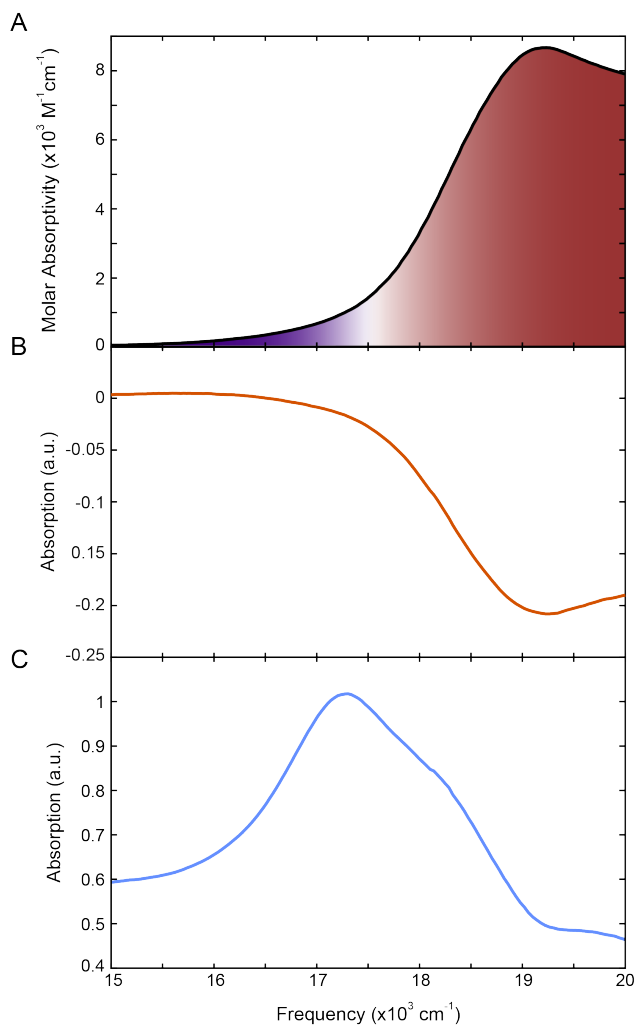
1.3 Spectroelectrochemical data

Figure S4: Spectroelectrochemical data of $[Fe(bpy)_3]^{2+}$. (A) Static absorption spectrum of $[Fe(bpy)_3]^{2+}$ in acetonitrile with the ^{1}MLCT and ^{3}MLCT states denoted in red and purple, respectively. (B) Oxidative spectroelectrochemical spectrum of $[Fe(bpy)_3]^{2+}$ in acetonitrile shows the reduced MLCT absorption when an electron is removed from the metal. (C) Reductive spectroelectrochemical spectrum of $[Fe(bpy)_3]^{2+}$ in acetonitrile shows the spectral signature of the radical bipyridine anion.

2   Kinetic Fits of 2D Spectra

2.1   Biexponential fitting of the on-diagonal and cross peak

For Figures 2, 3, and 5, the traces plotted for the on-diagonal peak and cross peak were fit from $T = 47$ fs up to $T = 1$ ps to the following biexponential fit:

$$\text{Fit} = -a_1 \exp\left(-t/\tau_1\right) + a_2 \exp\left(-t/\tau_2\right) \qquad\qquad \text{(Equation S1)}$$

where t is the waiting time, a_1 is the weighting factor of the short-time rise (Rise Weight), τ_1 is the lifetime of the rise (Rise Time), a_2 is the weighting factor of the long-time decay (Decay Weight), and τ_2 is the timescale of the decay (Decay Time). As reported, a_1 and a_2 were normalized such that $a_1 + a_2 = 1$. These fit parameters are reported in Tables S1 and S2.

Table S1: Extracted components from the biexponential fit of the on-diagonal peak of $[\text{Fe(bpy)}_3]^{2+}$ in methanol, 1-propanol, acetonitrile, and butyronitrile.

Solvent	Rise Weight (a.u.)	Rise time (ps)	Decay Weight (a.u.)	Decay Time (ps)
Methanol	0.52 ± 0.08	0.0325 ± 0.006	0.49 ± 0.08	17.616 ± 3.049
1-Propanol	0.73 ± 0.10	0.024 ± 0.010	0.27 ± 0.10	55.462 ± 32.924
Acetonitrile	0.62 ± 0.12	0.025 ± 0.005	0.38 ± 0.12	51.718 ± 22.652
Butyronitrile	0.35 ± 0.10	0.070 ± 0.005	0.65 ± 0.10	13.331 ± 5.598

Table S2: Extracted components from the biexponential fit of the cross peak of $[\text{Fe(bpy)}_3]^{2+}$ in methanol, 1-propanol, acetonitrile, and butyronitrile.

Solvent	Rise weight (a.u.)	Rise time (ps)	Decay Weight (a.u.)	Decay Time (ps)
Methanol	0.87 ± 0.06	0.028 ± 0.010	0.13 ± 0.06	23.668 ± 4.631
1-Propanol	0.95 ± 0.05	0.013 ± 0.004	0.05 ± 0.05	14.545 ± 6.920
Acetonitrile	0.85 ± 0.09	0.021 ± 0.006	0.15 ± 0.09	3.465 ± 1.110
Butyronitrile	0.78 ± 0.17	0.046 ± 0.018	0.22 ± 0.17	12.323 ± 8.861

To accurately fit the rise, the biexponential fit was performed for a truncated range ($T = 47$ fs - 1 ps). For more accurate fitting of the decay, see below (where the biexponential fit was performed over the range $T = 47$ fs - 700 ps).
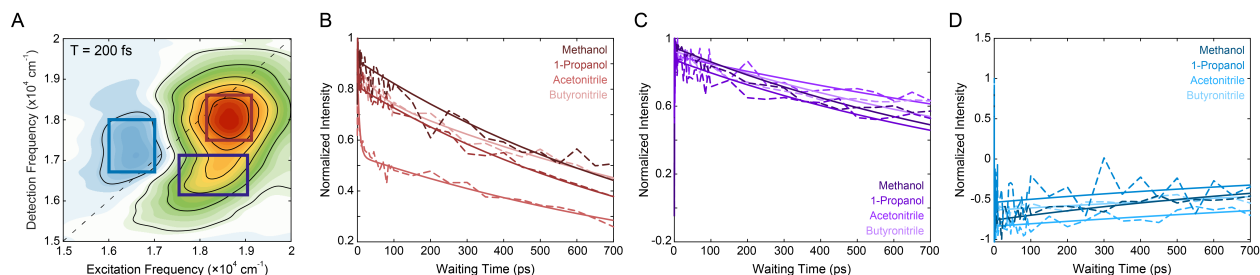
Figure S5: Long-timescale dynamics. (A) 2DES spectrum of $[Fe(bpy)_3]^{2+}$ in methanol at $T = 200$ fs. The blue, red, and purple boxes correspond to the regions that are integrated over for the ESA, on-diagonal GSB, and cross peak traces, respectively. (B) Intensity traces (dashed lines) of the on-diagonal GSB peak over population time T with their respective biexponential fits (solid lines) in methanol, 1-propanol, acetonitrile, and butyronitrile. (C) Intensity traces (dashed lines) of the cross peak over population time T with their respective biexponential fits (solid lines) in the same set of solvents. (D) Intensity traces (dashed lines) of the ESA peak over population time T with their respective biexponential fits (solid lines) in the same set of solvents.

For Figure S5, the traces plotted for the on-diagonal peak and cross peak were fit from $T = 47$ fs up to $T = 700$ ps to Equation S1. As with that seen for Figures 2, 3 and 5, the biexponential fit here is also fit to a rise (coefficient a_1, timescale τ_1) and a decay (coefficient a_2, timescale τ_2). Because of the relatively fast rise (and comparatively small number of data points associated with the rise when accounting for T times up to 700 ps), a_1 and τ_1 are less precise than the values extracted from the fit up to 1 ps shown in Figure S6 and reported in Tables S1 and S2. The incorporation of long waiting times allows the most precise fit of the nanosecond decay time. The fit models the decay more accurately by incorporating the later time points. Therefore, only the τ_2 time is reported here for each peak in Table S4.

Table S3: Reported decay times from a biexponential fit of traces in Figure S5.

Solvent	[1]MLCT GSB decay (ps)	[3]MLCT GSB decay (ps)	ESA decay (ps)
Methanol	965	1064	1215
1-Propanol	918	1093	1380
Acetonitrile	1096	1837	2642
Butyronitrile	1250	1294	2282
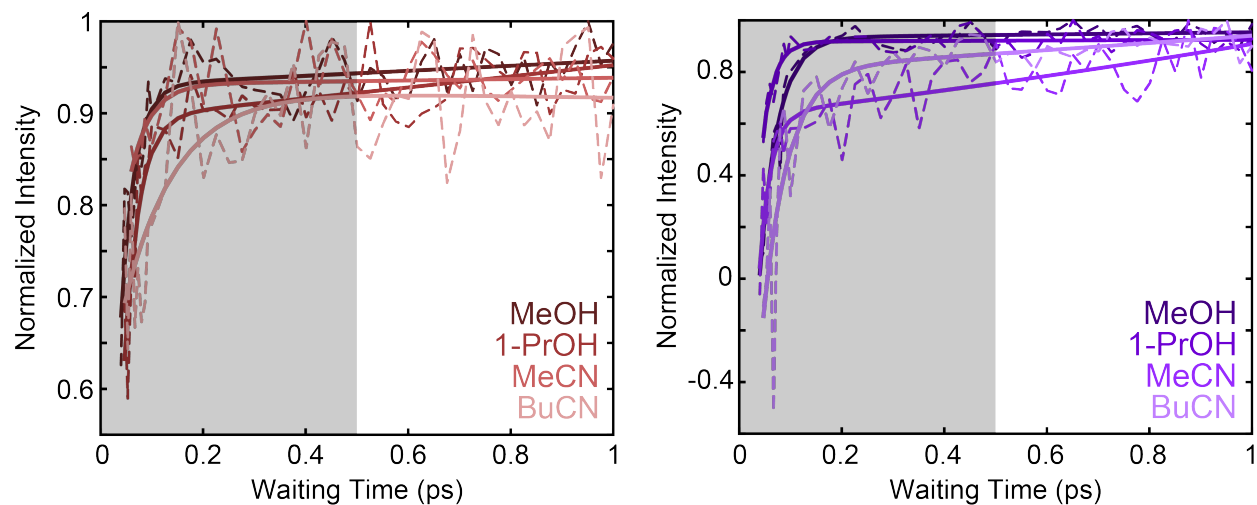
Figure S6: Full visualization of biexponential fits. Biexponential fit of the positive peak (Figures 2 and 3) and cross peak (Figure 5) in methanol are cutoff at 500 fs (gray area) to better visualize the rise. The fit itself is performed for data points up to 1 ps, the averaged trace of which is fully visualized here in methanol, 1-propanol, acetonitrile, and butyronitrile (left - positive peak, right - cross peak).
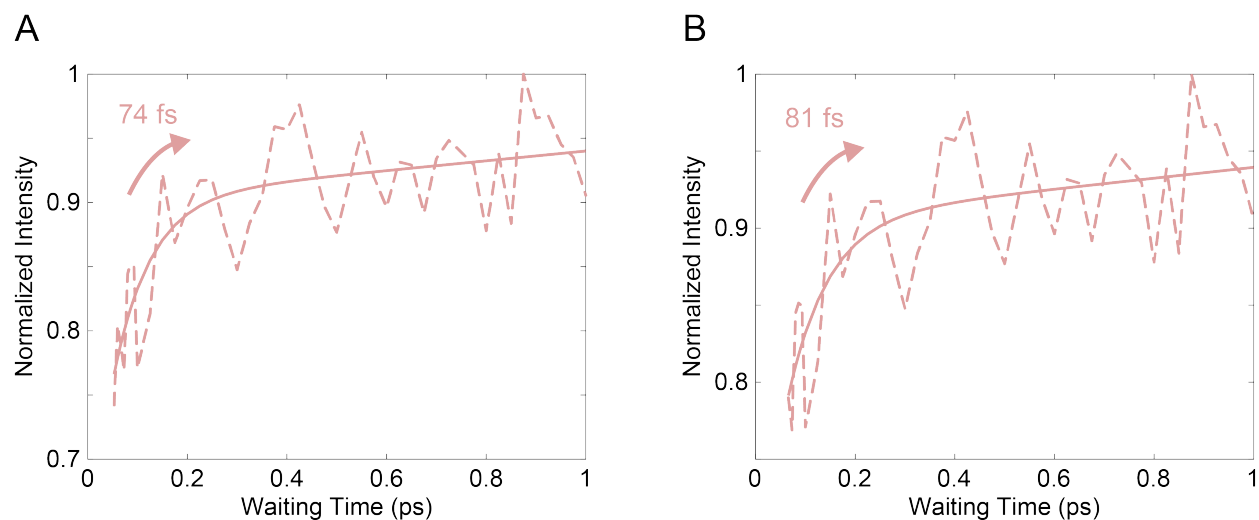
Figure S7: Rise lifetime of $[Fe(bpy)_3]^{2+}$ in butyronitrile with different start points. As the rise of the butyronitrile ^{1}MLCT GSB/SE peak was relatively shallow, different start points were tested to ensure the robustness of the rise. Both of the cutoff points exclude the nonresonant response, which has a lifetime of ~25 fs (Figure S2). (A) ^{1}MLCT GSB/SE peak trace in butyronitrile (dashed) with a cutoff at 50 fs. The fit of this rise was determined to be 74 fs. (B) ^{1}MLCT GSB/SE peak trace in butyronitrile (dashed) with a cutoff at 60 fs. The fit of this rise was determined to be 81 fs.

2.2 Reproducibility of [1]MLCT GSB/SE and cross peak rise times
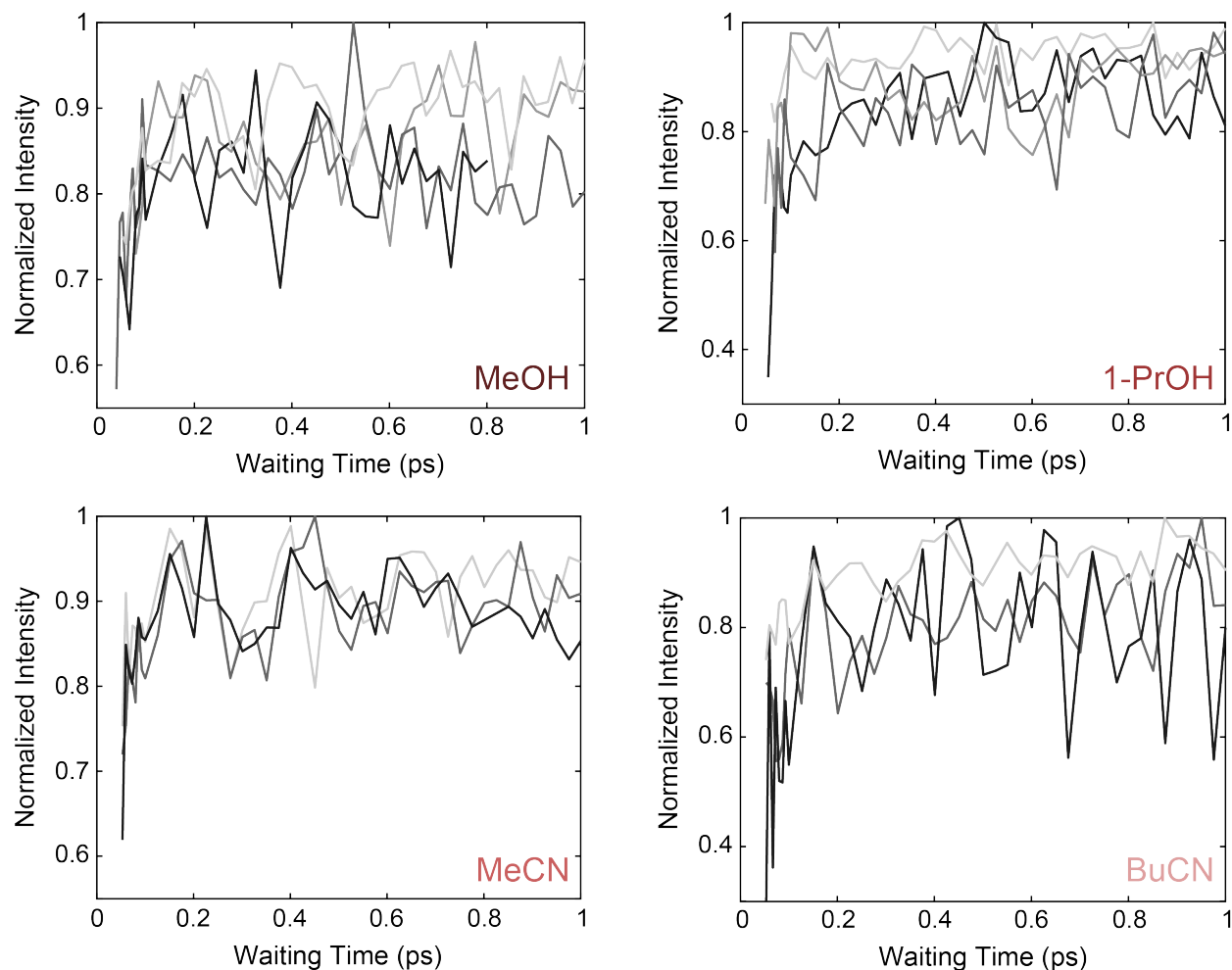
Figure S8: Reproducibility of the [1]MLCT GSB/SE kinetics in different solvents. Individual traces taken from each 2DES dataset (including replicates) in Methanol, 1-Propanol, acetonitrile, and butyronitrile of the [1]MLCT GSB/SE peak. These traces are then averaged, shown in Figure S6 (and Figure 2B of the main text for methanol), and their rises averaged for the extracted rise lifetimes in Figures 3C.
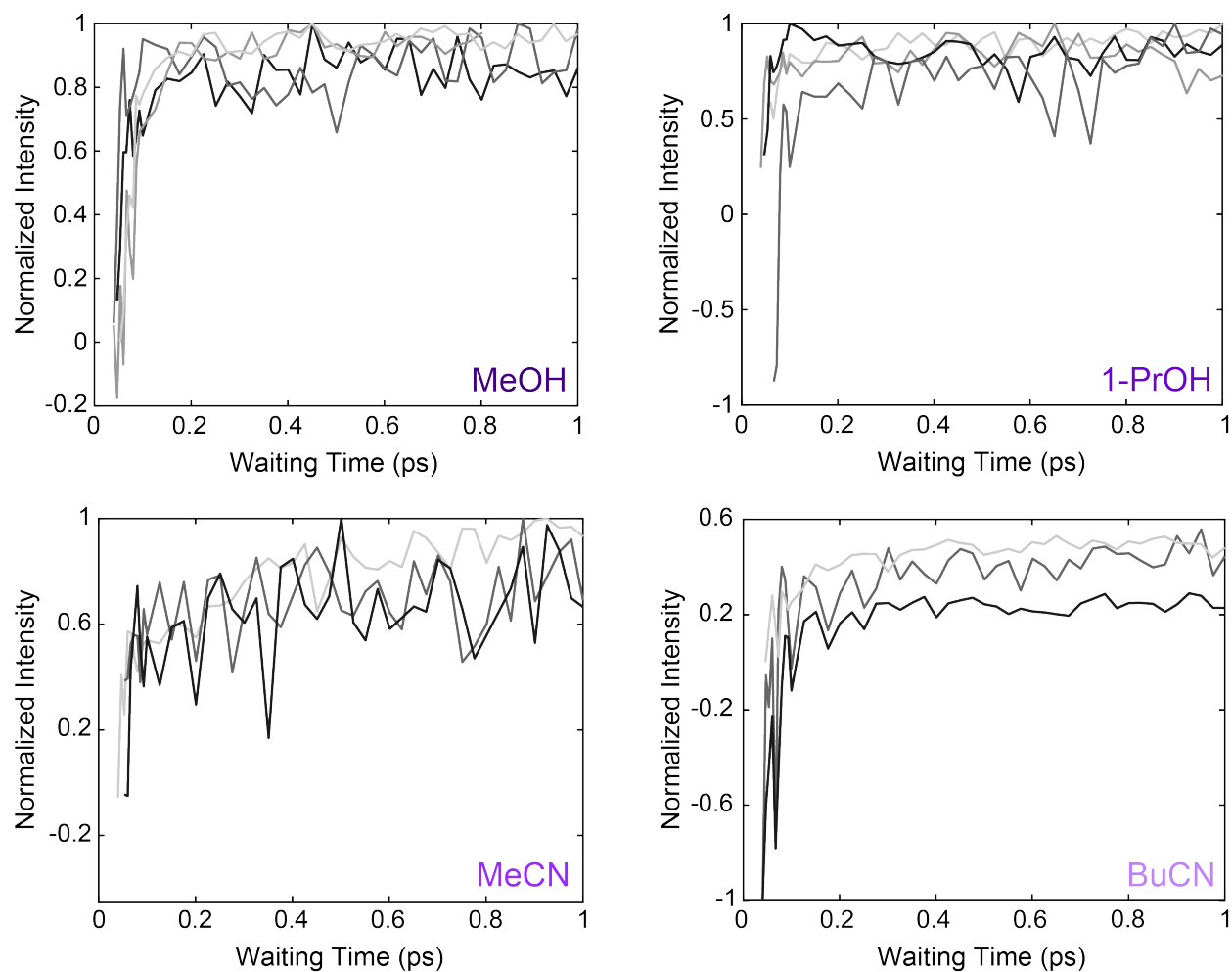
Figure S9: Reproducibility of the ^{1}MLCT$\rightarrow^3$MLCT cross peak kinetics in different solvents. Individual traces taken from each 2DES dataset (including replicates) in methanol, 1-propanol, acetonitrile, and butyronitrile of the ^{1}MLCT$\rightarrow^3$MLCT cross peak. These traces are then averaged, shown in Figure S6 (and in Figure 5B of the main text for methanol), and their rises averaged for the extracted rise lifetimes in Figure 5C.
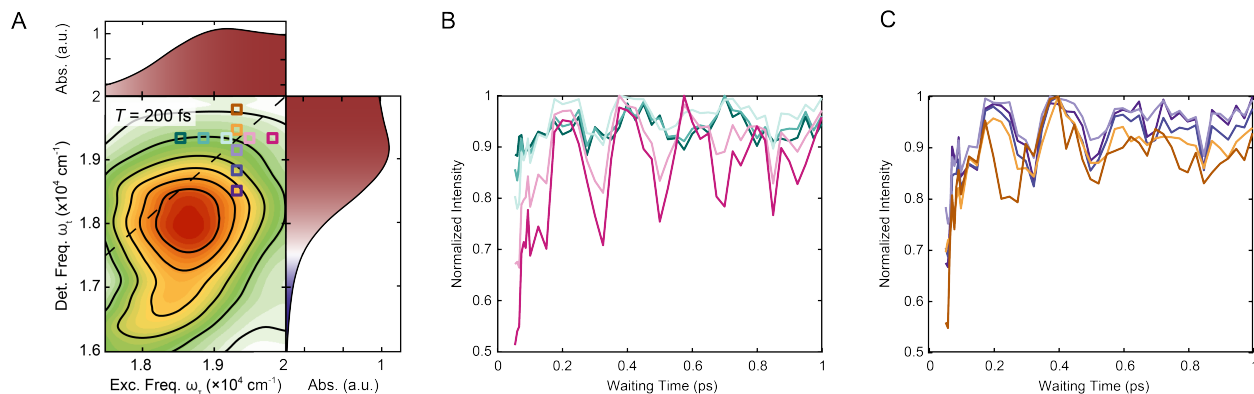
Figure S10: Spectral dependence of kinetics within the on-diagonal peak. Selected trace lineouts of $[Fe(bpy)_3]^{2+}$ in methanol over waiting times T (denoted in Figure S10A) plotted throughout the cross peak region that is integrated over for kinetic trace seen in Figure 2B of the main text. The traces plotted in Figure S10B are at different excitation frequencies, with the detection frequency held at $\omega_t = 19,250$ cm^{-1}, while those plotted in Figure S10C are taken at different detection frequencies, with the excitation frequency held at $\omega_t = 19,200$ cm^{-1}. Note the integrated region for kinetic analysis is not at the maximum of the peak to avoid effects of the nonresonant response at early timescales (Figure S2).All traces are integrated over 100 cm^{-1} in both excitation and emission frequencies, and show no major changes through the region.

2.3 Fourier filter analysis
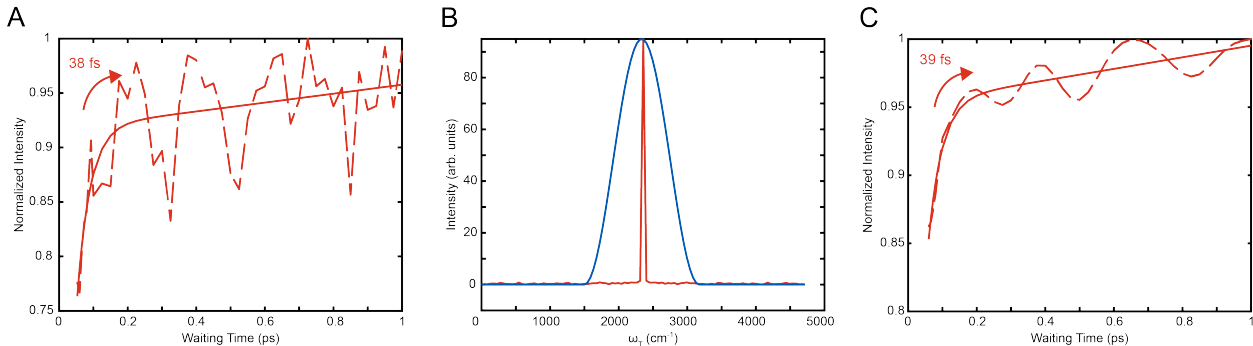
Figure S11: Fourier filter applied onto kinetic trace for the [1]MLCT GSB/SE peak. (A) Plot of a kinetic trace for the [1]MLCT GSB/SE peak in methanol (dashed line) along with its biexponential fit (solid line). The rise time was analyzed to be 38 fs. (B) The fourier transform of the kinetic trace in (A) (red line), along with the filter (blue line). A hann function centered on the primary peak is used as the filter window. (C) The resulting filtered trace (dashed line) along with its corresponding biexponential fit (solid line). The rise lifetime was similar to that pre-filter at 39 fs. Therefore, the unfiltered data were analyzed for all sets.

Fourier filtering is a signal processing method[S1,S2] that, in this case, is applied to eliminate oscillatory components to better isolate the initial rise in signal at early waiting times. Using this method, the kinetic trace (Figure S11A, dashed line) of the signal that has oscillations was Fourier-transformed with respect to the waiting time (T), creating a plot in the frequency domain as a function of ω_T (Figure S11B, red line). As a result, the x-axis in Figure S11B still corresponds to waiting time, but in the units of wavenumbers, reflecting the $T \to \omega_T$ transformation. In the frequency domain, contributions to the initial rise have the highest amplitude, whereas noise and oscillatory contributions are much smaller. A windowing function centered on the largest peak was applied to the Fourier-transformed signal, preserving the initial rise and removing noise and oscillations. To minimize edge effects, a Hann window was used. The post-windowed signal was then inverse Fourier transformed back into the time domain (i.e., the waiting time), yielding a trace with suppressed oscillations and noise. Because the window function filters out both noise components and oscillatory components (as both exist outside of the filtering window), the filtered trace will

also exhibit reduced oscillatory structure.

For the purposes of this study, the fourier filter allowed for a better fit of the rise, though the lifetime extracted were largely the same, as seen in the comparison between the fits of Figure S11A and C. Therefore, it was determined that the oscillatory features in the [1]MLCT GSB/SE peak do not greatly alter the quality of the biexponential fit, and the rise lifetimes extracted therefore primarily influenced by the underlying population dynamics.

3 Oscillatory Behavior
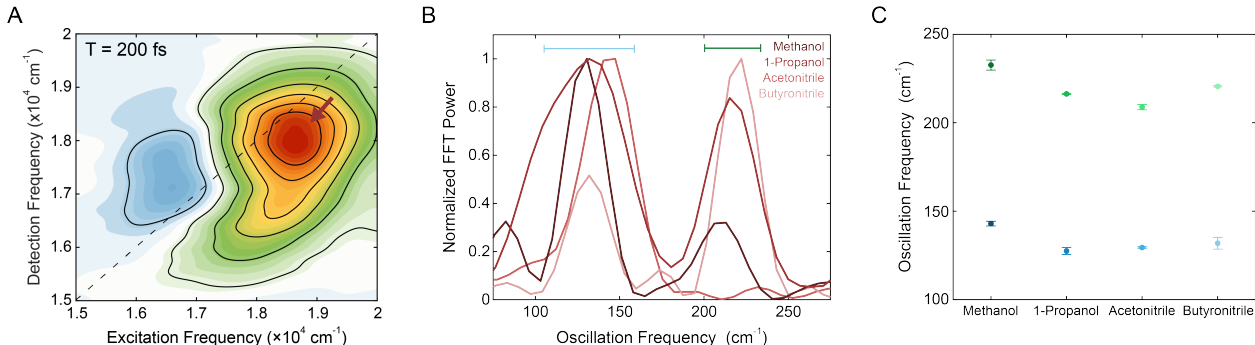
Figure S12: Oscillatory behavior of the on-diagonal GSB peak. (a) Representative 2DES spectrum taken in methanol at $T = 200$ fs. The red arrow corresponds to the peak from which the oscillatory behavior is observed. (b) FFT power spectrum (normalized) of the residuals of the on-diagonal GSB peak in methanol, 1-propanol, acetonitrile, and butyronitrile (red lines). The presence of two primary oscillations, denoted and light blue and green, are observed. (c) The oscillation frequency of the maximum of the FFT power spectrum for the two primary oscillations plotted in blue and green, respectively, from datasets in the same set of solvents. These two oscillations correspond to $N-Fe-N$ bending ($\sim 127 - 157$ cm^{-1}) and $Fe-N$ stretching (~ 185–280 cm^{-1}) modes.[S3,S4]

Table S4: Oscillations reported from Figure S12.

Solvent	$N-Fe-N$ Bend (cm^{-1})	$Fe-N$ Stretch (cm^{-1})
Methanol	129.4 ± 0.4	209 ± 1
1-Propanol	127 ± 2	216.3 ± 0.4
Acetonitrile	143 ± 1	233 ± 3
Butyronitrile	132 ± 3	220.5 ± 0.4

Oscillatory behavior in $[Fe(bpy)_3]^{2+}$ were determined through fourier transformation of the residuals from the biexponential fit. This can be subject to the analysis procedure and the fit itself. Namely, oscillatory modes can either be extracted by fourier transforming the residuals of the fits from individual datasets or by first averaging the traces from individual datasets and then fourier transforming the resulting residuals from the fit (the latter of which was reported). Depending on the analysis method, the frequencies of the oscillatory modes were shifted by tens of wavenumbers, but trends were preserved and the frequencies extracted still fell within the range of established $[Fe(bpy)_3]^{2+}$ oscillatory modes.

4 Moment of Inertia Calculations

In Figure 3C, the moment of inertia (I) for each nitrile solvent is plotted. This was calculated assuming a rigid rotor approximation using the following equation:

$$I = \mu R^2 \qquad \text{(Equation S2)}$$

where μ is the reduced mass between the carbon chain and the cyano group (calculated using the atomic weight of the components, in atomic units) and R is the length of the carbon chain. For R, the C−C bond length was assumed to be the length of the C−C bond in ethane (1.535 Å)[S5] and the C−C−C bond angle was assumed to be that in propane (111.5 °).[S5] Since the carbon chain for longer solvents is kinked, the true distance was calculated as

$$\sin(\frac{111.5}{2}) \cdot 1.535\text{Å} = 1.269\text{Å}. \qquad \text{(Equation S3)}$$

Table S5: Moment of inertia calculated for nitrile solvents, plotted in Figure 3C.

Solvent	I (a.u.×Å^2)
Acetonitrile	67.980
Butyronitrile	396.280
Pentanenitrile	689.624
Hexanenitrile	1065.924

5 Identification and Assignment of the Cross Peak
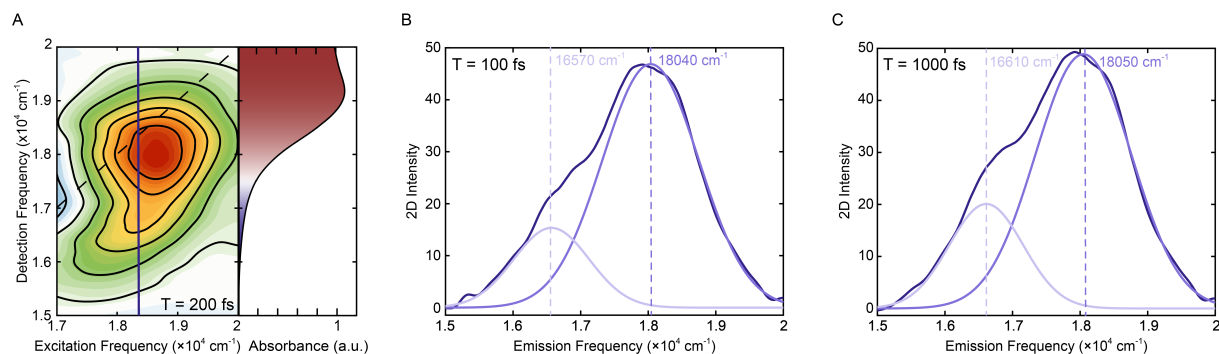
Figure S13: Gaussian decomposition of spectra at $\omega_\tau = 18,300$ cm^{-1}. Vertical slice at $\omega_\tau = 18,300$ cm^{-1} (shown over a reproduction of the 2DES spectrum at $T = 200$ fs in (A)) at $T = 100$ fs (B) and $T = 1000$ fs (C) reveal two unique peaks, one corresponding to the ^{1}MLCT GSB transition ($\omega_t \sim 18,050$ cm^{-1}) and the other corresponding to the off-diagonal positive peak ($\omega_t \sim 16,590$ cm^{-1}).
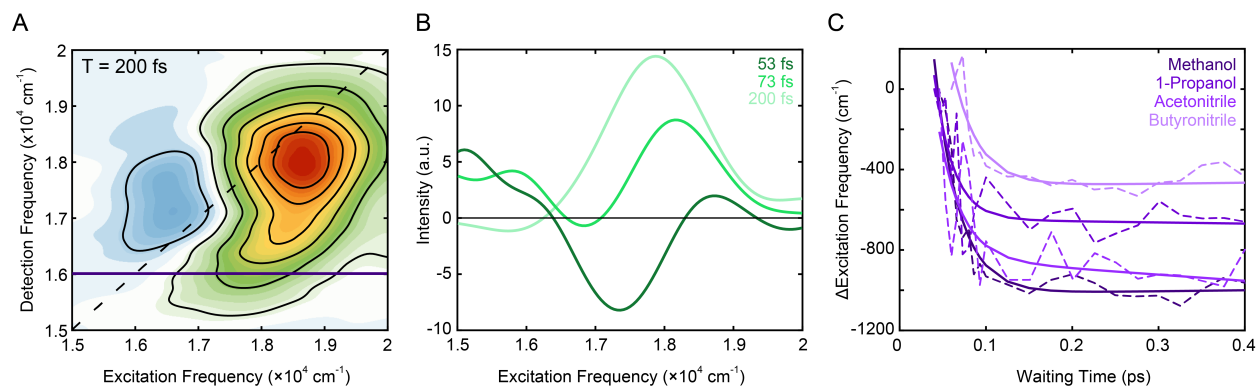
Figure S14: Shift in excitation frequency of the cross peak. (A) The center of the off-diagonal peak was determined using a gaussian fit of the horizontal slice extracted from the spectra at $\omega_t = 16,000$ cm^{-1} at waiting times T. (B) The horizontal slice at select T times is shown. (C) The peak center was then plotted as change from the first time point (ΔExcitation Frequency) as a function of waiting time T and the shift was fitted using a biexponential model with the timescale of the shift determined to be $\sim$20-30 fs.
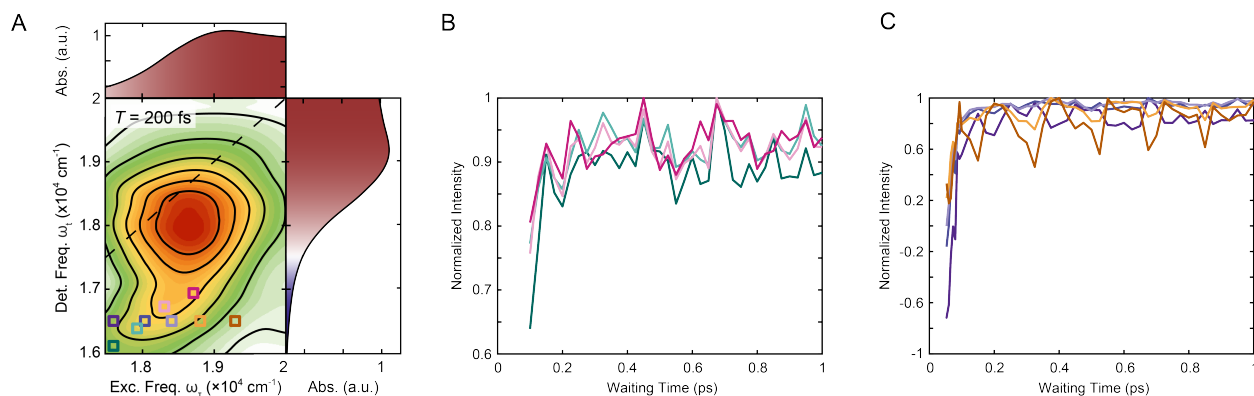
Figure S15: Spectral dependence of kinetics within the cross peak. Selected lineouts of [Fe(bpy)$_3$]$^{2+}$ in methanol over waiting time (denoted in Figure S15A) plotted throughout the cross peak region that is integrated over for kinetic traces seen in Figure 5B of the main text. The traces plotted in Figure S15B are taken along the diagonal of the cross peak, while those plotted in Figure S15C are taken at different excitation frequencies, with the detection frequency held at $\omega_t = 16,500$ cm^{-1}. All traces are integrated over 100 cm^{-1} in both excitation and emission frequencies, and show no major changes through the region.

6 Relative Intensities of Peaks in Spectra
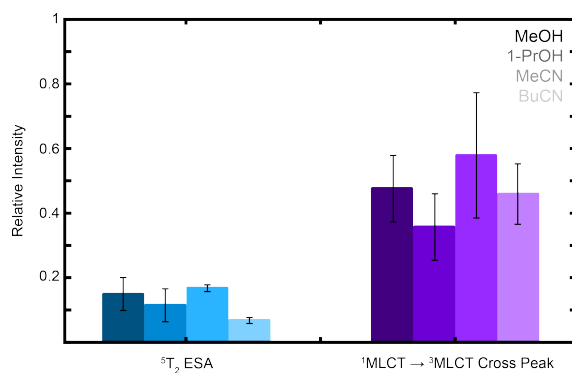
Figure S16: Relative intensities of cross peak and ESA peak. The relative intensity (taken as an absolute value) of the $^5T_2$ ESA peak (blue) and the ^{1}MLCT $\rightarrow$ ^{3}MLCT cross peak (purple) shown as a fraction of the on-diagonal ^{1}MLCT GSB/SE peak (set to 1).

7 Extended Studies on Nitriles

To confirm that the solvent dependence of the rise of the ^{1}MLCT GSB/SE peak in nitriles, additional studies were performed on heavier nitrile solvents to confirm the correlation of the trend with that of the inertial response time of the solvent. In addition to the ^{1}MLCT GSB/SE peak rise lifetime plotted in the main text, additional information (namely, relative intensities and cross peak rise times) are shown below.
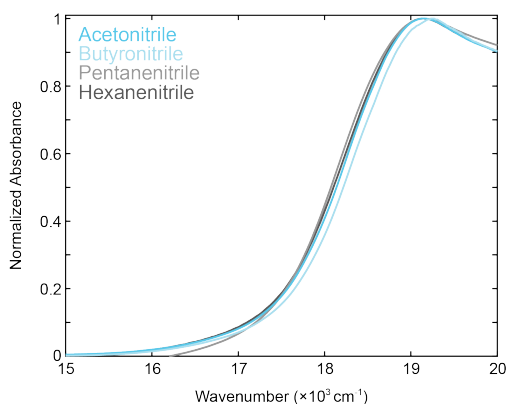
Figure S17: Linear absorption spectra of $[Fe(bpy)_3]^{2+}$ in acetonitrile, butyronitrile, pentanenitrile, and hexanenitrile (blue and gray lines), showing minor solvatochromic effects.
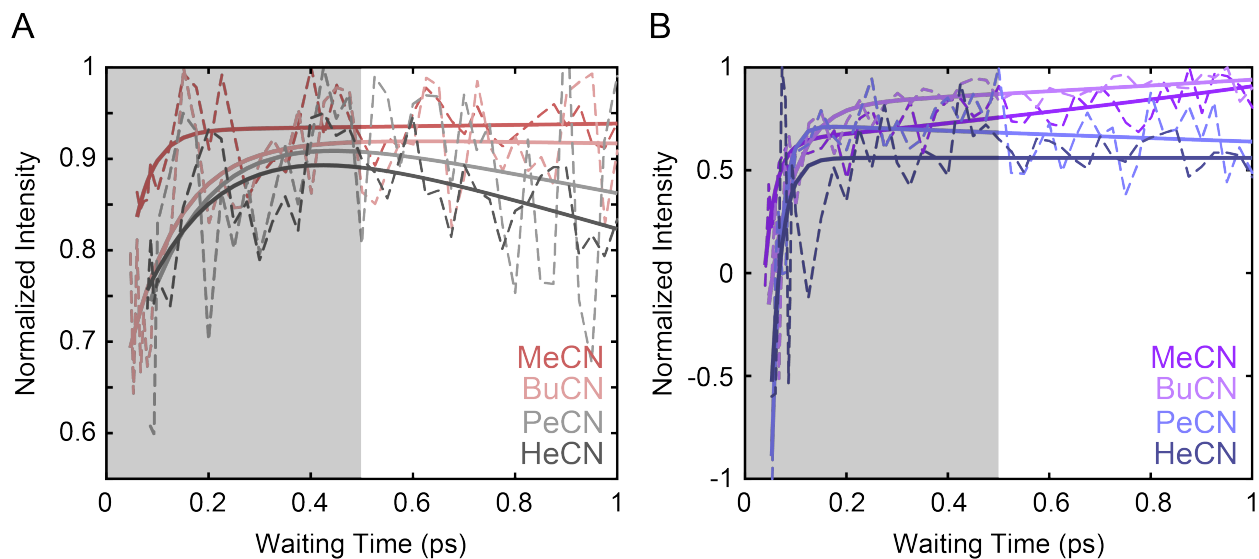
Figure S18: Full visualization of biexponential fits - nitriles. The biexponential fit to extrapolate the bpy$^{\bullet-}$ decay lifetime and the intersystem crossing lifetime is performed for data points up to 1 ps, fully visualized here ((A) positive peak, (B) cross peak). The first 500 fs are grayed to aid in visual comparisons to Figure S6 and Figures 2B and 5B in the main text.

The fit values for the ^{1}MLCT GSB/SE peak and cross peak of pentanenitrile and hexanenitrile using the equation in Equation S1 are shown below.

Table S6: Extracted components from the biexponential fit of the on-diagonal peak of [Fe(bpy)$_3$]$^{2+}$ in pentanenitrile and hexanenitrile.

Solvent	Rise Weight (a.u.)	Rise time (ps)	Decay Weight (a.u.)	Decay Time (ps)
Pentanenitrile	0.34 ± 0.08	0.14 ± 0.04	0.66 ± 0.08	$(1.13 \pm 1) \times 10^{12}$
Hexanenitrile	0.19 ± 0.03	0.18 ± 0.02	0.08 ± 0.03	$(2.7 \pm 1.1) \times 10^{10}$

Table S7: Extracted components from the biexponential fit of the on-diagonal peak of [Fe(bpy)$_3$]$^{2+}$ in pentanenitrile and hexanenitrile.

Solvent	Rise weight (a.u.)	Rise time (ps)	Decay Weight (a.u.)	Decay Time (ps)
Pentanenitrile	0.98 ± 0.02	0.021 ± 0.003	0.018 ± 0.003	$(7.1 \pm 1.8) \times 10^{10}$
Hexanenitrile	0.97 ± 0.02	0.024 ± 0.003	0.03 ± 0.02	$(9.1 \pm 8.9 \times) 10^8$
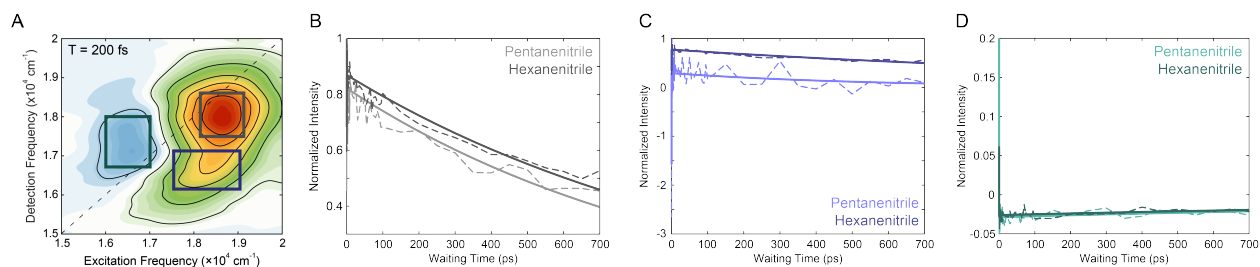
Figure S19: Long-timescale dynamics for additional nitrile studies. (A) Reference 2DES spectrum of $[\text{Fe(bpy)}_3]^{2+}$ in methanol at $T = 200$ fs. The blue, gray, and purple boxes correspond to the regions that are integrated over for the ESA, on-diagonal GSB, and cross peak traces, respectively. (B) Intensity traces (dashed lines) of the on-diagonal GSB peak over population time T with their respective biexponential fits (solid lines) in pentanenitrile and hexanenitrile. (C) Intensity traces (dashed lines) of the cross peak over population time T with their respective biexponential fits (solid lines) in the same set of solvents. (D) Intensity traces (dashed lines) of the ESA peak over population time T with their respective biexponential fits (solid lines) in the same set of solvents.

Table S8: Reported decay times from a biexponential fit of traces in Figure S19.

Solvent	^{1}MLCT GSB decay (ps)	^{3}MLCT GSB decay (ps)	ESA decay (ps)
Pentanenitrile	961	549	2317
Hexanenitrile	1095	1588	2380
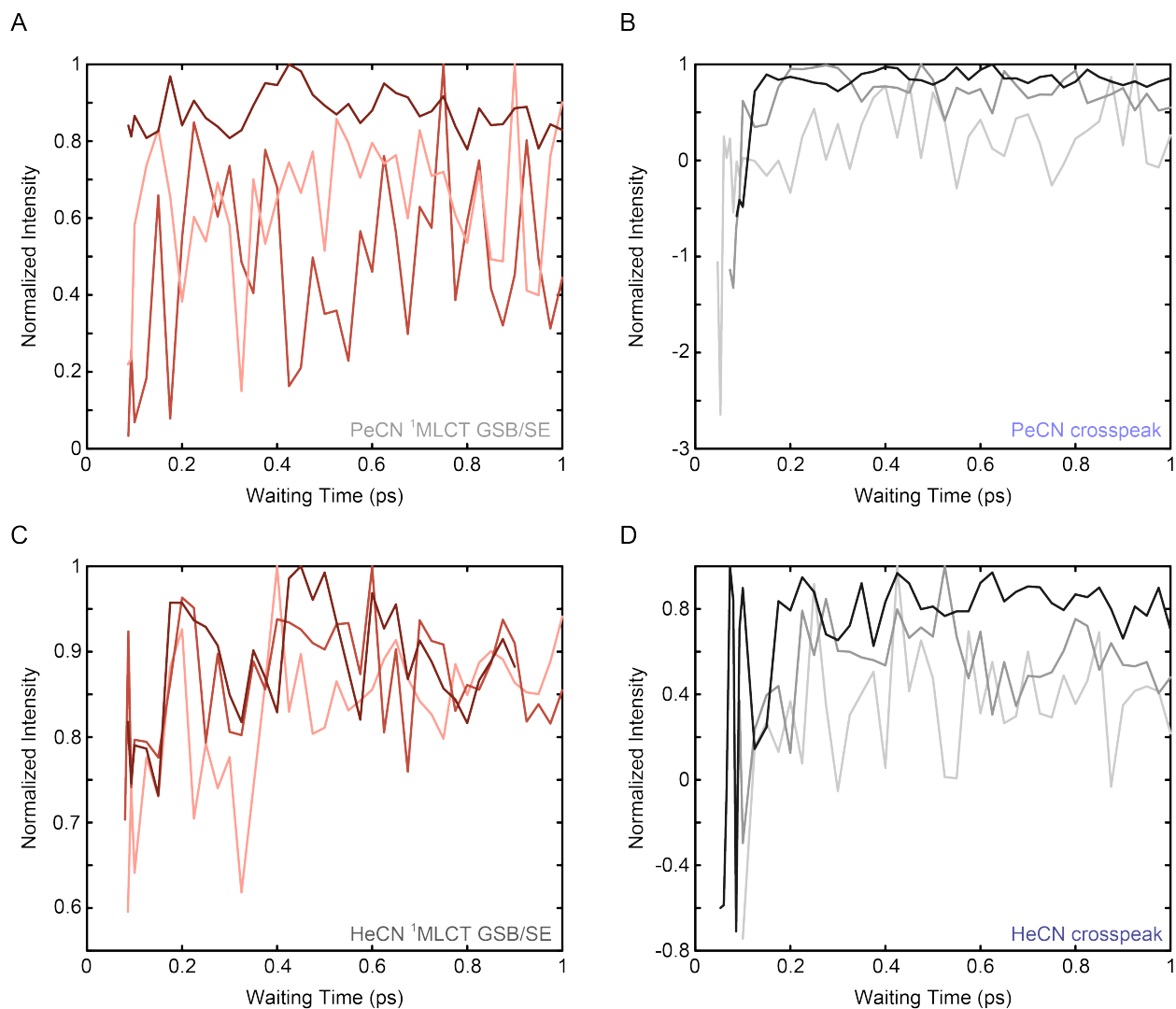
Figure S20: Reproducibility of the ^{1}MLCT GSB/SE kinetics (A,C) ^{1}MLCT→^{3}MLCT cross peak kinetics (B,D) in pentanenitrile and hexanenitrile. Individual traces taken from each 2DES dataset (including replicates) in each solvent. These traces are then averaged, shown in Figure S18, and their rises averaged for the extracted rise lifetimes in Table 1 and in Figure 3C in the main text.

7.1 Impurities in Propionitrile

The impurities unique to the chemical processing of propionitrile led to difficulties in performing 2DES experiments in the solvent. Below is a brief description of the difficulties, along with a procedure to filter impurities of propionitrile for reference in future studies.
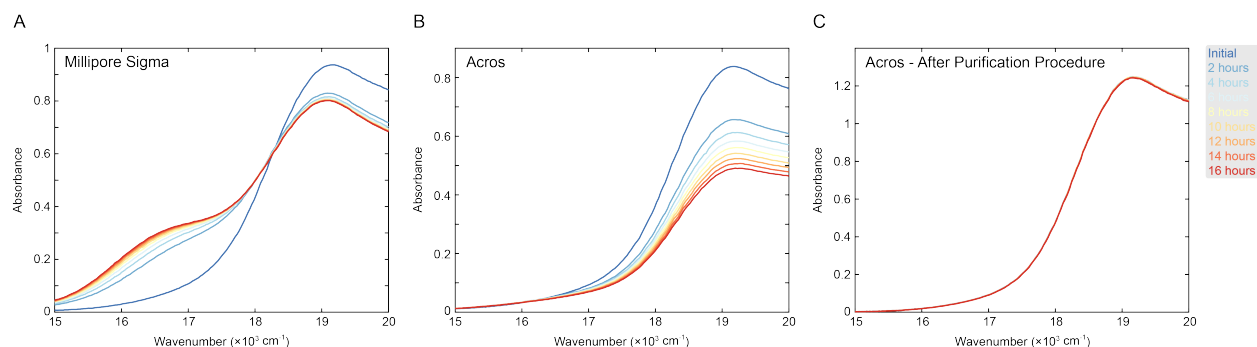
Figure S21: (A) Degradation of $[\mathrm{Fe(bpy)_3}]^{2+}$ in propionitrile from Millipore Sigma. (B) Degradation of $[\mathrm{Fe(bpy)_3}]^{2+}$ in propionitrile from Acros. (C) Degradation of $[\mathrm{Fe(bpy)_3}]^{2+}$ in propionitrile from Acros purified using the procedure described in the text below.

$[\mathrm{Fe(bpy)_3}]^{2+}$ proved to be unstable in propionitrile, likely due to the presence of isonitriles in solvent.[S6] Figure S21A and B shows the degradation over the course of 16 hours in reagent-grade propionitrile from Millipore Sigma and Acros (Thermo Scientific), respectively. The degradation occurs primarily within the first two hours.

A simple procedure of stirring propionitrile in neutral alumina overnight followed by filtering the solvent through neutral alumina or celite produces a solvent of high enough purity to minimize degradation (Figure S21C).

8 Global Analysis of 2DES Spectra
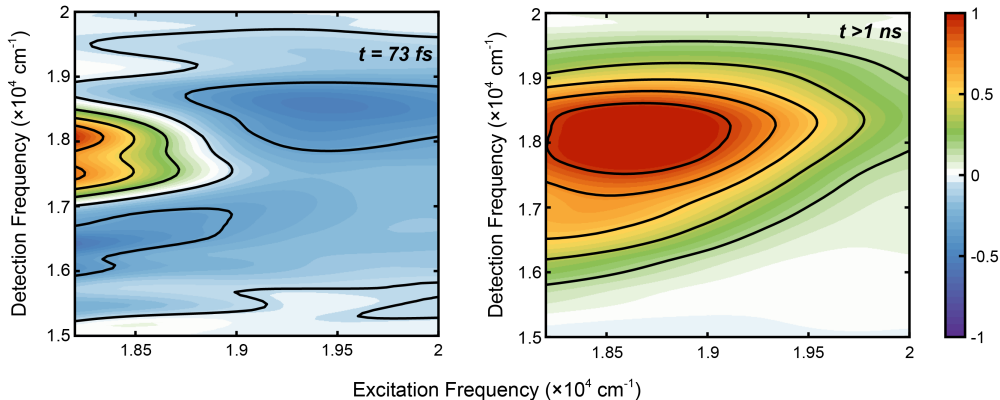
Figure S22: Global analysis of 2DES spectra. (Left) The EAS of the first state observed, with a decay timescale of 73 fs. (Right) The EAS of the second state observed with a decay timescale greater than 1 ns. Both spectra are normalized to the maxiumum of the left spectrum.

To confirm the dynamics established throughout the main text, global analysis of the 2DES data, specifically the butyronitrile sample, were conducted using the approach described by *Volpato, et. al.*[S7] Here, a sequential kinetic model was used with two states: a first, fast-decay state, and a second, long-time state (that decays on the timescale of charge recombination of the complex). Adding additional states caused non-physical results. Therefore, the lifetime of the cross peak and that of the ondiagonal peak were not separable via global analysis, as their timescales were too similar. Furthermore, to minimize the effect of the nonresonant response signal that occurs at early timescales, primarily at $\omega_\tau < 18,100$ cm^{-1} (Figure S2), the spectra were windowed from $\omega_\tau = 18,100 - 20,000$ cm^{-1}. Furthermore, to more accurately capture early timescale dynamics, the spectra were only analyzed from $T = 47 - 1,500$ fs. The results presented in Figure S22 are therefore the Evolution-Associated Spectra (EAS) generated from the model.

The EAS on the left corresponds to the early-time state that decays with a lifetime of 73 fs. It primarily includes population from the ^{1}MLCT GSB/SE peak, with some minor contributions from the ^{1}MLCT$\rightarrow^3$MLCT intersystem crossing contributions. The lifetime is

consistent with the timescales obtained from kinetic analysis of the ^{1}MLCT GSB/SE and ^{1}MLCT$\rightarrow$^{3}MLCT ISC peaks separately for this dataset (70 and 80 fs, respectively). This further confirms that the two lifetimes are difficult to isolate using global analysis methods due to similar kinetic lifetimes and relatively close spectral features. Therefore, kinetic analysis of individual peaks are presented in the main text.

The EAS on the right corresponds to the second state that grows in with a 73 fs lifetime and decays on the charge recombination timescale (>1 ns). This spectrum reflects depopulation of the ^{1}MLCT GSB/SE peak and the ^{3}MLCT GSB/SE peak.

9   Contributions of Different Transitions to Absorption Spectra
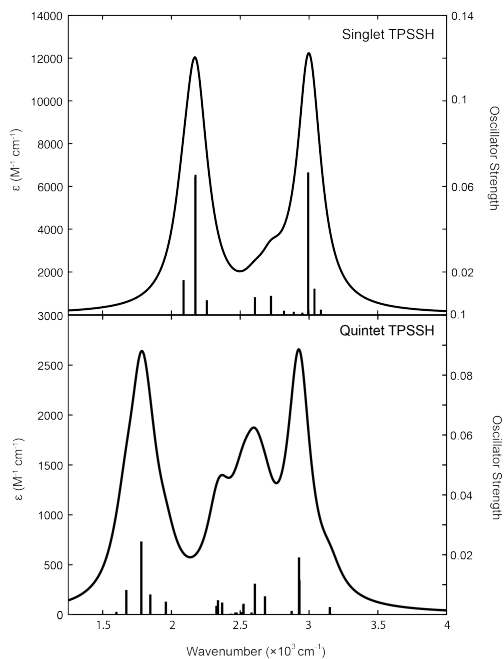
Figure S23: Calculated UV-Vis spectra of $[Fe(bpy)_3]^{2+}$, showing the oscillator strengths and associated molar absorptivity for $[Fe(bpy)_3]^{2+}$ obtained at the TPSSH/6-311G*,SDD level of theory in acetonitrile. (Top) Calculated singlet excitations (black sticks) and their associated molar absorptivity (black line) for $[Fe(bpy)_3]^{2+}$ obtained from a TD-DFT calculation utilizing a ground state singlet as a reference state. (Bottom) Calculated transitions (black sticks) and their associated molar absorptivity (black line) for $[Fe(bpy)_3]^{2+}$ obtained from a TD-DFT calculation utilizing the lowest-energy quintet state as a reference.
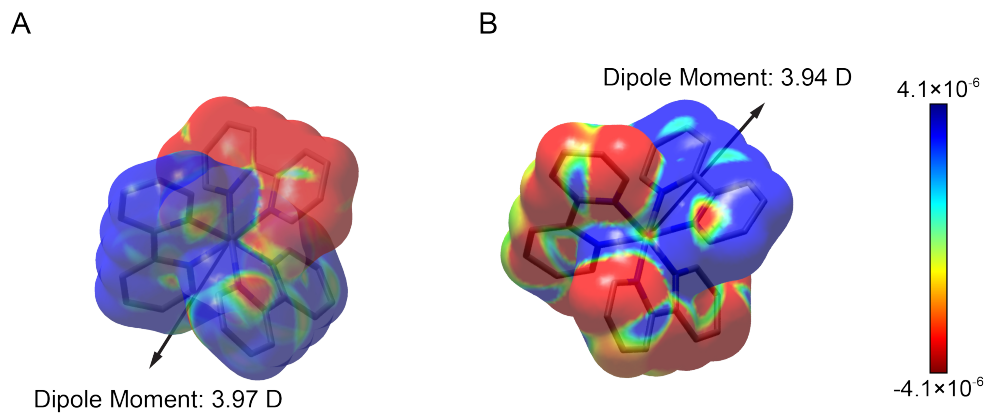
Figure S24: Electron density difference surface between the ground and the degenerate initially-excited ^{1}MLCT state densities (isovalue = 0.0004 electrons/a.u.^{3}). The ^{1}MLCT states correspond to a doubly degenerate transition at 21,832 cm^{-1} . Red values indicate an increase in the excited-state electron density relative to the ground state (particle), blue values indicate a decrease (hole). The excited-state dipole moments: 3.97 (A) and 3.94 (B) Debye is depicted by an arrow pointing in the positive direction.
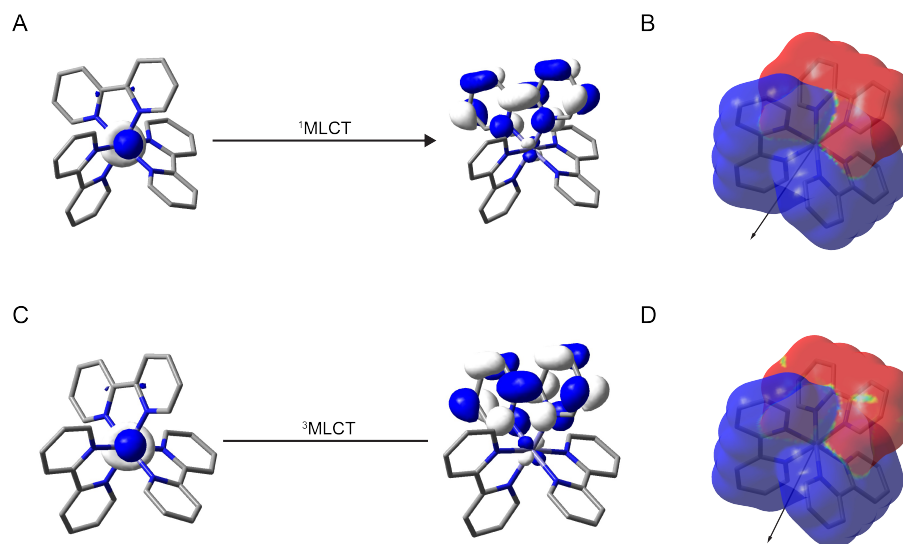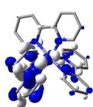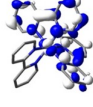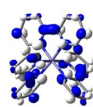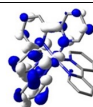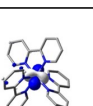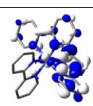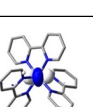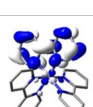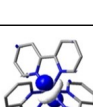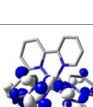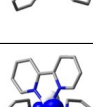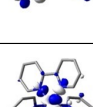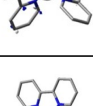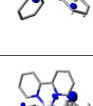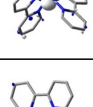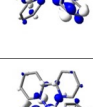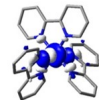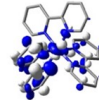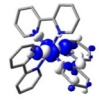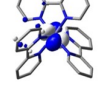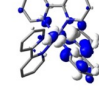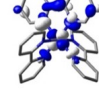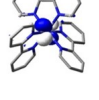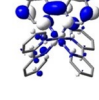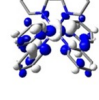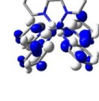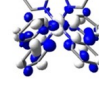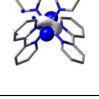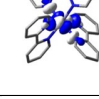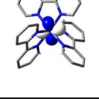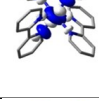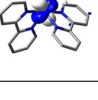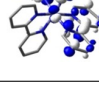
Figure S25: Molecular orbital contributions of the fully optimized lowest energy ^{1}MLCT (A) and ^{3}MLCT (C) states predicted by TD-DFT. Electron density difference surface between the ground and the fully optimized lowest-energy MLCT states densities (isovalue = 0.0004 electrons/a.u.^{3}) are also displayed: (B) ^{1}MLCT and (D) ^{3}MLCT. Red values indicate an increase in the excited-state electron density relative to the ground state (particle), blue values indicate a decrease (hole). The excited-state dipole moments are 9.0 (^{1}MLCT) and 6.7 (^{3}MLCT) Debye, which are depicted by an arrow pointing in the positive direction.

Table S9: Vertical excitation energies and natural transition orbitals (NTO) analysis for the singlet states at TPSSH/6-311G*, SDD level using ^1A as the reference state

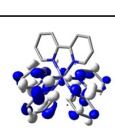| #	Excitation Energy (nm)	Oscillator Strength	NTO coeff.	Hole	Particle	Assignment	Dipole (noneq.)
1	514.55	0.0004	0.96597			MLCT	4.81
2	514.44	0.0004	0.96603			MLCT	4.80
3	490.67	0.0003	0.97554			MLCT	0.03
4	485.35	0.0001	0.49253			MLCT	0.09
			0.48338			MLCT	
5	479.56	0.0127	0.46668			MLCT	2.74
			0.29277			MLCT	
			0.24092			d-d	
6	479.52	0.0127	0.43283			MLCT	2.75
			0.36558			MLCT	

			0.20212			d-d	
7	465.19	0.0032	0.59108			MLCT	2.52
			0.38940			d-d	
8	465.07	0.0032	0.65139			MLCT/d-d	2.52
			0.25215			MLCT/d-d	
9	458.16	0.0664	0.74682			MLCT	3.97
			0.21685			MLCT/d-d	
10	458.04	0.0662	0.74691			MLCT	3.94
			0.20844			MLCT	
11	453.06	0.0000	0.50742			d-d	0.03
			0.49466			d-d	
12	428.65	0.0000	0.44396			MLCT	0.01
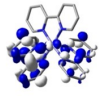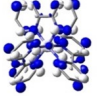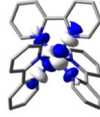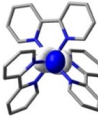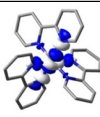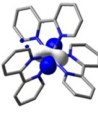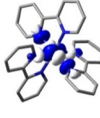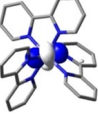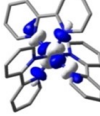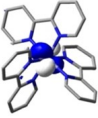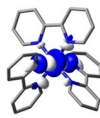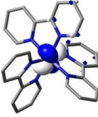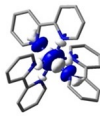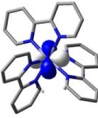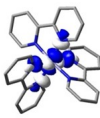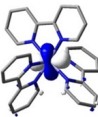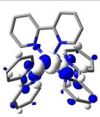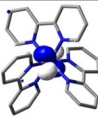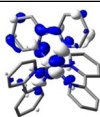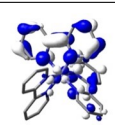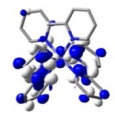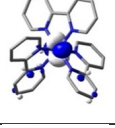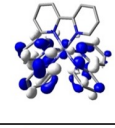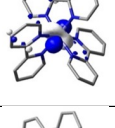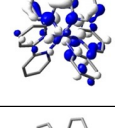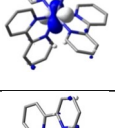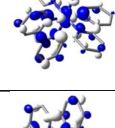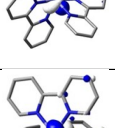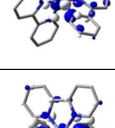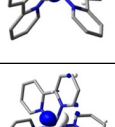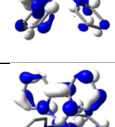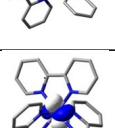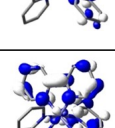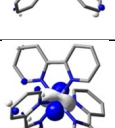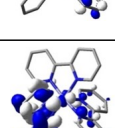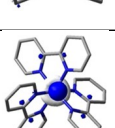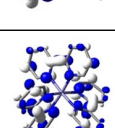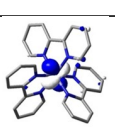
			0.44327		MLCT	
			0.10551		MLCT	

Table S10: Vertical excitation energies and natural transition orbitals (NTO) analysis for the triplet states at TPSSH/6-311G*, SDD level using ^1A as the reference state

#	Excitation Energy (nm)	Oscillator Strength	NTO coeff.	Hole	Particle	Assignment
1	928.02	0.000	1.02			d-d
2	927.12	0.000	1.02			d-d
3	788.08	0.000	0.57			d-d
			0.56			d-d
4	628.97	0.000	0.59			d-d
			0.38			d-d
5	628.20	0.000	0.59			d-d
			0.38			d-d
6	622.89	0.000	0.54			d-d
			0.5			MLCT

7	550.69	0.000	0.8			MLCT
			0.18			MLCT
8	550.17	0.000	0.79			MLCT
			0.19			MLCT
9	531.23	0.000	0.52			MLCT
			0.48			MLCT
10	524.30	0.000	0.59			MLCT
			0.34			MLCT
11	524.05	0.000	0.60			MLCT
			0.33			MLCT
12	510.56	0.000	0.83			MLCT
13	490.38	0.000	0.44			MLCT
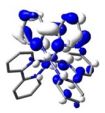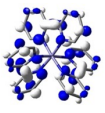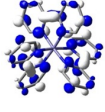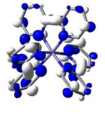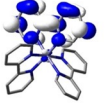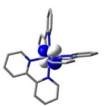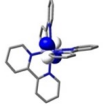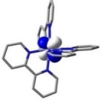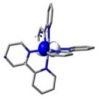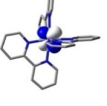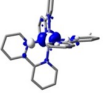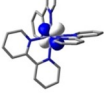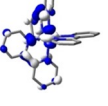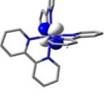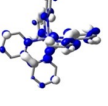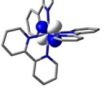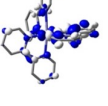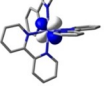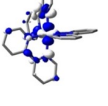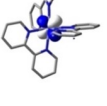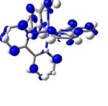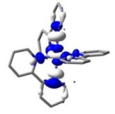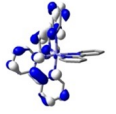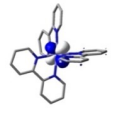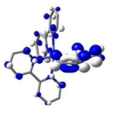
			0.43			MLCT
			0.13			MLCT
14	477.06	0.000	0.97			MLCT
15	476.76	0.000	0.97			MLCT
16	403.09	0.000	0.84			MLCT

Table S11: Vertical excitation energies and natural transition orbitals (NTO) analysis for the quintet states at TPSSH/6-311G*, SDD level using ^5T as reference state.

#	Excitation Energy (nm)	Oscillator Strength (Dipole Moment)	NTO coeff.	Hole	Particle	Assignment	S^2
1	2962.57	0.0008 (1.27)	1.35			d-d	6.018
2	2297.69	0.0006 (1.58)	1.17			d-d	6.033
3	624.96	0.0009 (0.20)	1.00			d-d	6.232
4	598.15	0.0082 (4.36)	1.00			MLCT d-d	6.525
5	561.39	0.0244 (1.58)	0.99			MLCT d-d	7.027
6	541.55	0.0067 (2.02)	0.98			MLCT d-d	6.933
7	510.29	0.0043 (3.25)	1.00			MLCT d-d	6.477
8	429.73	0.0029 (2.21)	0.89			MLCT d-d	6.963

9	427.70	0.0048 (4.94)	0.86			MLCT	6.412
			0.11			MLCT	

References

(S1) Rabiner, L. R.; Gold, B. *Theory and application of digital signal processing*; 1975.

(S2) de Beer, A. G. F.; Chen, Y.; Scheu, R.; Conboy, J. C.; Roke, S. Analysis of Complex Spectra Using Fourier Filtering. *The Journal of Physical Chemistry C* **2013**, *117*, 26582–26587.

(S3) Lawson Daku, L. M. Spin-state dependence of the structural and vibrational properties of solvated iron(ii) polypyridyl complexes from AIMD simulations: aqueous [Fe(bpy)3]Cl2, a case study. *Phys. Chem. Chem. Phys.* **2018**, *20*, 6236–6253.

(S4) Alexander, B. D.; Dines, T. J.; Longhurst, R. W. DFT calculations of the structures and vibrational spectra of the [Fe(bpy)3]2+ and [Ru(bpy)3]2+ complexes. *Chem. Phys.* **2008**, *352*, 19–27.

(S5) Pauling, L.; Brockway, L. O. Carbon—Carbon Bond Distances. The Electron Diffraction Investigation of Ethane, Propane, Isobutane, Neopentane, Cyclopropane, Cyclopentane, Cyclohexane, Allene, Ethylene, Isobutene, Tetramethylethylene, Mesitylene, and Hexamethylbenzene. Revised Values of Covalent Radii. *Journal of the American Chemical Society* **1937**, *59*, 1223–1236.

(S6) Tessensohn, M. E.; Ng, S. J.; Chan, K. K.; Gan, S. L.; Sims, N. F.; Koh, Y. R.;

Webster, R. D. Impurities in Nitrile Solvents Commonly Used for Electrochemistry, and their Effects on Voltammetric Data. *ChemElectroChem* **2016**, *3*, 1753–1759.

(S7) Volpato, A.; Bolzonello, L.; Meneghin, E.; Collini, E. Global analysis of coherence and population dynamics in 2D electronic spectroscopy. *Opt. Express* **2016**, *24*, 24773–24785.